Versatile Activity of a Copper(II) Complex Bearing a N4-Tetradentate Schiff Base Ligand with Reduced Oxygen Species

Micaela Richezzi, Joaquín Ferreyra, Juan Puzzolo, Lisandro Milesi, Claudia M Palopoli, Diego M Moreno, Christelle Hureau, Sandra R Signorella

Versatile Activity of a Copper(II) Complex Bearing a N_4-Tetradentate Schiff Base Ligand with Reduced Oxygen Species

Micaela Richezzi,[a] Joaquín Ferreyra,[a] Juan Puzzolo,[a] Lisandro Milesi,[a] Claudia M. Palopoli,[a] Diego M. Moreno,[a] Christelle Hureau,[b] and Sandra R. Signorella*[a]

[a] M. Richezzi, J. Ferreyra, J. Puzzolo, L. Milesi, Prof. Dr. C. M. Palopoli, Prof. Dr. D. M. Moreno, Prof. Dr. S. R. Signorella
IQUIR (Instituto de Química Rosario), Facultad de Ciencias Bioquímicas y Farmacéuticas
CONICET – Universidad Nacional de Rosario
Suipacha 531, S2002LRK Rosario, Argentina
E-mail: signorella@iquir-conicet.gov.ar

[b] Dr. C. Hureau
LCC (Laboratoire de Chimie de Coordination)
CNRS, Université de Toulouse
205 Route de Narbonne, 31077 Toulouse, France

Supporting information for this article is given via a link at the end of the document.

Abstract: The reactivity of the Cu(II) complex of N,N'-bis(pyridin-2-ylmethylene)propane-1,3-diamine (py_2pn), $[Cu(py_2pn)(ClO_4)_2]$, toward $O_2^{\bullet-}$ and H_2O_2 has been examined. The complex reacts with $O_2^{\bullet-}$ with fast second order kinetics, k_{McF} = 4.05 x 10^6 M^{-1} s^{-1}, employing the Cu(II)/Cu(I) couple proved by spectroscopic detection of the reduced form at low temperature. At -40ºC in DMF, the reaction of the complex with H_2O_2/Et_3N yields an stable end-on Cu(II)-hydroperoxide, with k^{OOH} = 0.31 min^{-1}, the formation of which has been established by DFT calculations, electronic and EPR spectra. At room temperature, the end-on Cu(II)-hydroperoxide reacts with a second Cu(II) complex to evolve O_2, with k_{CAT} = 83.2 M^{-2} s^{-1}. The Cu(II)-hydroperoxide can mediate phenol oxidation, probably through a trigonal bipyramidal ternary transition state based on DFT analysis, favored over catalase activity when low proportion of catalyst is used. In these reactions, structural constraints imposed by the ligand distort the coordination geometry of the metal and controls reactivity.

Introduction

Cu-dependent metalloenzymes, such as oxygenases or oxidases, carry out a rich redox chemistry involving reaction with O_2 or reduced forms, which has inspired the development of synthetic protocols for the functionalization of organic molecules under environmentally benign conditions.[1,2] The mode of action of copper in these enzymes and synthetic complexes depends on the nature of the copper-oxygen intermediates involved in the oxidative transformations.[3] Copper complexes of active oxygen species such as superoxide, hydroperoxide and high-valent copper oxo species have been proposed as key intermediates in these biological and chemical oxidations.[4-8] However, although a number of well-characterized and even structurally defined $LCu(II)O_2$ species involved in a variety of such copper catalyzed oxidations have been described, and some of them stabilized,[9-13] much is still unknown about the fundamental chemistry of many of them. The reactivity of L–Cu(II)–($O_2^{\bullet-}$)/L–Cu–OOH species has mostly been studied with tripodal tetradentate N_4 donor ligands,[14-17] while copper Schiff-base compounds, especially with ligands bearing N_2O_2-donor sets, have extensively been studied as galactose oxidase mimics and catalysts in chemical oxidation processes.[17-24]

In the Cu(II)/Cu(I) redox chemistry, the metal activity is strongly affected by the environment around the metal center because electron transfer involves changes in the coordination number and geometry.[25-26] When switching between both oxidation states small structural reorganization is usually required for fast electron transfer, which depends on the rigidity/flexibility of the ligand.[27,28] In copper complexes of the N,N'-bis(2-pyridinylmethylen)alkane-1,n-diamine family, the Cu(II)/Cu(I) redox potential and geometry can be tuned by the length of the alkyl chain between the two imino N-atoms.[29] Therefore, Cu(II) complexes of N_4-tetradentate Schiff base ligands are an excellent platform for testing reactivity with superoxide and hydrogen peroxide and evaluating their antioxidant/pro-oxidant activity. To our knowledge, little is known about intermediate $[LCuO_2(H)]^+$ species formed in the reaction of this kind of complexes with either superoxide or peroxide, or catalytic active species involved in oxidation reactions. Here, we report kinetic, spectroscopic and theoretical studies on the reaction of $[Cu(py_2pn)(ClO_4)_2]$ (py_2pn = N,N'-bis(2-pyridinylmethylen)propane-1,3-diamine) with superoxide and hydrogen peroxide and the ability of this complex to catalyze phenol oxidation by H_2O_2, aimed at examining how this ligand influence the reactivity of the copper center and the nature of copper-oxygen intermediate species involved in the redox pathways.

Results and Discussion

Characterization of the complex in the solid state and solution

The powdered Cu(II) complex, $[Cu(py_2pn)(ClO_4)_2]$, was obtained by adding $NaClO_4$ to a 1:1 mixture of $Cu(OAc)_2$ and py_2pn in methanol. Crystals of the complex were obtained by slow diffusion of ether into an acetonitrile solution. The compound crystallized in the C2/c space group, as previously reported by Ghosh & col.[30] but marginally different from the structure reported by Jäntti & col. for crystals obtained from acetonitrile as the sole solvent.[31] The lattice consists of discrete $[Cu(py_2pn)(ClO_4)_2]$ molecules with the hexacoordinated Cu(II) center adopting a typical Jahn−Teller

distortion, where the N_4-donor atoms of the tetradentate ligand are disposed in the equatorial plane describing a slightly distorted square-planar geometry, with the apical positions occupied by two capping perchlorate anions. In the crystal, the complex possesses short Cu-N_{py} and Cu-N_{im} distances of 2.024 and 1.995 Å, respectively, and longer Cu-O distances of 2.475Å (Table S1). The optimized structure of $[Cu(py_2pn)(ClO_4)_2]$ obtained by DFT calculations (shown in Figure 1(a)) is consistent with the geometrical parameters of the complex in the crystal, with bond distances and angles given in Table S1. Interestingly, computational modeling of the complex using DMF as implicit solvent, predicts that, in solution, one perchlorate dissociates and the pentacoordinated $[Cu(py_2pn)(ClO_4)]^+$ complex adopts a distorted square-pyramidal geometry with perchlorate at the apical position and one N_{im} shifted downward the equatorial plane of Cu(II), as shown in the optimized structure of $[Cu(py_2pn)(ClO_4)]^+$ illustrated in Figure 1(b), with bond distances and angles listed in Table S1.

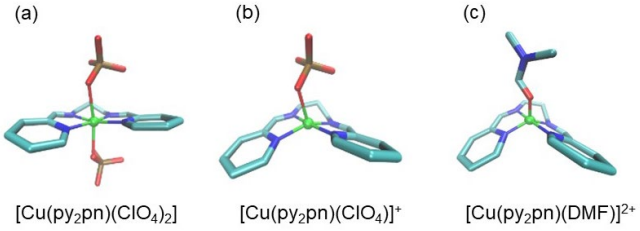

Figure 1. Optimized geometries for $[Cu(py_2pn)(ClO_4)_2]$ (a); and $[Cu(py_2pn)ClO_4]^+$ (b) and $[Cu(py_2pn)DMF]^{2+}$ (c) in DMF as implicit solvent

X-band electron paramagnetic resonance (EPR) spectra (Figure 2(a)) registered at 120 K on powdered and DMF or DMSO frozen solutions of the complex display axial signals characteristic of Cu(II) in tetragonal geometry with a d_{x2-y2} ground state ($g_e < g_x \sim g_y < g_z$). Furthermore, in frozen solutions, hyperfine splitting due to the interaction of the unpaired electron with the copper nucleus (I = 3/2) was observed in the parallel direction of the g-tensor, while superhyperfine splitting due to bound nitrogen atoms was not detected in any solvent. Spectral parameters in frozen DMF and DMSO solutions are $g_{\|}$ = 2.24, $A_{\|}$ = 184 x 10^{-4} cm^{-1} and $g_{\perp}$ = 2.06, somewhat different from $g_{\|}$ = 2.22 and $g_{\perp}$ = 2.07 of the solid, indicating a more distorted geometry in the solution. This is consistent with structural reorganization of the complex calculated by DFT in DMF as implicit solvent, where the lowest-energy species corresponds to $[Cu(py_2pn)(ClO_4)]^+$. The formation of $[Cu(py_2pn)(ClO_4)]^+$ was also observed by ESI-MS, where this species (m/z 414.0) is present in either protic and aprotic solvents (shown in methanol in Figure 2(b)). In the positive mode ESI-mass spectrum, besides the major peaks observed at m/z = 315.1 (100%) and 157.5 (38%), corresponding to $[Cu(py_2pn)]^+$ and $[Cu(py_2pn)]^{2+}$, respectively, two other peaks are present at m/z 347.1 (14%) and 414.0 (15%) whose mass and isotope distribution patterns correspond to $[Cu(py_2pn)(CH_3OH)]^+$ and $[Cu(py_2pn)ClO_4]^+$, respectively. The relative proportion of $[Cu(py_2pn)]^+$ and $[Cu(py_2pn)]^{2+}$ species depends on the cone voltage employed in the ESI-MS measurements.[32] Higher cone voltages resulted in a lowering of $[Cu(py_2pn)]^{2+}$ abundance, while $[Cu(py_2pn)]^+$ increased concomitantly with the increase of the intensity of ions of smaller m/z ratio. Thus, the proportion of oxidized and reduced species in the mass spectra are related to gas-phase reactions in the electrospray and not related to the presence of Cu(I) complex in the solution. The same species are observed when the complex is dissolved in DMF or DMSO and then diluted with methanol.

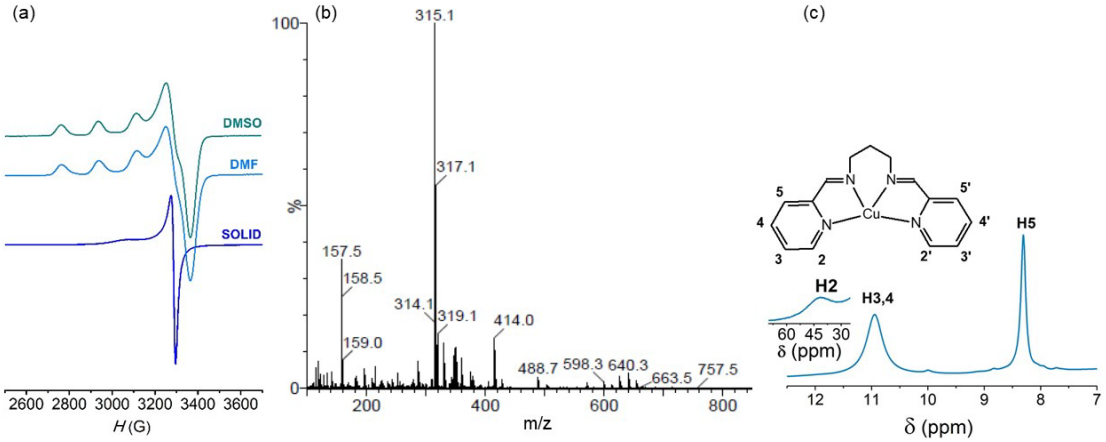

Figure 2. (a) X-band EPR spectra of powdered $[Cu(py_2pn)(ClO_4)_2]$ and its DMF or DMSO frozen solutions. ν = 9.51 GHz, T = 120 K, microwave power = 0.5 mW. (b) ESI-mass spectrum of $[Cu(py_2pn)]^{2+}$ in methanol. Cone voltage = 30 V. (c) ^{1}H NMR spectrum of $[Cu(py_2pn)]^{2+}$ (14 mM) in D_6-DMSO.

The UV-vis spectrum of the complex supports the proposed geometry for the complex in solution, as it exhibits a broad low-intensity d-d band centered at 626 nm typical of Cu(II) in square-pyramidal geometry.[33] The absence of bands at longer wavelengths precludes the presence of species with trigonal-bipyramidal metal coordination geometry.[34] Additionally, the complex exhibits a very strong absorption in the UV region where π-π* and ligand-to-metal charge transfer transitions overlap. In DMF, replacement of perchlorate by the solvent molecule can occur giving an even more distorted geometry, with one N_{py} and one N_{im} moving down from the solvent-copper bond as shown in Figure 1(c) and Table S1 for the optimized geometry of the complex with DMF coordinated to Cu(II). Both $[Cu(py_2pn)(ClO_4)]^+$ and $[Cu(py_2pn)DMF]^{2+}$ forms probably coexist in solution. For simplicity, hereafter the complex in solution will be referred as $[Cu(py_2pn)]^{2+}$.

The complex was also characterized by ^{1}H NMR in DMSO solution. The spectrum, shown in Figure 2 (c), exhibits three isotropically shifted NMR resonances ascribed to pyridine protons at 40.76 (H2/H2'), 10.84 (H3,H4/H3',H4') and 8.30 (H5/H5') ppm. This ^{1}H NMR spectral pattern indicates that protons belonging to both pyridine rings are not distinguished in the square-pyramidal geometry of the complex. Given the large relaxation values of the pyridine proton signals, distortions from this geometry are not resolved.[35] Besides, protons closer to the copper ion experience stronger paramagnetic effects and thus shorter longitudinal relaxation times and broader line width.[36] Therefore, the assignment of the resonance at 41 ppm to the α-proton of pyridine is consistent with its half-width and relatively large downfield shift compared to the other pyridine signals. Interestingly, the lack of signals attributable to the free ligand in the diamagnetic region of the spectrum of the complex, is an indication of the compound stability towards metal dissociation.

The redox potential of the complex is an important indicator of the electron-donor ability of the supporting ligand to control the reactivity of the metal center with reduced oxygen species. Cyclic voltammetry of the complex shows one quasi-reversible redox wave for the Cu(II)/Cu(I) couple, with $E_{1/2}$ = -39 mV *vs SCE* (Figure 3) The large peak separation (ΔE_p) of 200 mV suggests geometry changes during the redox process. Upon reduction, the py$_2$pn ligand is not flexible enough for Cu(I) to adopt a tetrahedral geometry, although Cu(II) reduction might be accompanied by solvent dissociation to afford Cu(I) in a flattened tetrahedral geometry. The ratio of the forward and reverse currents (I_{pa}/I_{pc}) for the quasi-reversible process is 0.85, and plots of either I_{pa} and I_{pc} vs $\upsilon^{1/2}$ are linear in the 10-200 mV s^{-1} range of scan rates (υ), in agreement with a diffusion-controlled process. Besides, the $w_{1/2}$ values of 118 mV in square-wave voltammetry experiments (pink line in Figure 3) confirm the redox process involves one electron. The lack of a re-dissolution peak upon anodic polarization scans excludes the presence of free copper, or the release of copper from the reduced complex.[37]

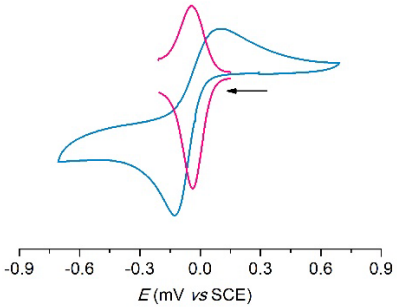

Figure 3. Cyclic (blue line) and square-wave (pink line) voltammogram of 1 mM complex in acetonitrile, 0.1M TBAPF$_6$ under argon, scan rate (CV): 50 mV/s, scan frequency (SWV): 2 Hz, T = 20 °C.

Reaction of [Cu(py$_2$pn)]$^{2+}$ with $O_2^{\bullet-}$

The catalytic disproportionation of $O_2^{\bullet-}$ requires reaction of both the reduced and oxidized forms of the catalyst with $O_2^{\bullet-}$. Therefore, the metal-centered redox potential is an important thermodynamic criterium for the superoxide dismutase (SOD) mimics activity.[38] When the redox potential of the metal center of the catalyst falls in between the $O_2^{\bullet-}$ one electron reduction ($E(O_2^{\bullet-}/H_2O_2)$ = 0.642 V, vs SCE at pH 7) and oxidation ($E(O_2/O_2^{\bullet-})$ = −0.404 V, vs SCE at pH 7), both reactions become thermodynamically favored. The potential of the Cu(II)/Cu(I) couple of the [Cu(py$_2$pn)]$^{2+}$ complex is within this potential range and is expected to exhibit SOD activity. Besides, the bending of py$_2$pn ligand in solution (Figure 1(b,c)), leads to a weakly coordinate exchangeable axial perchlorate or solvent molecule which favors substrate binding. The SOD activity of the complex was evaluated in phosphate buffer of pH 7.8 by an indirect method based on kinetic competition between nitro blue taetrazolium (NBT) and the complex for reacting with $O_2^{\bullet-}$.[39] In this assay, the SOD activity is inversely related to the amount of formazan, the purple product formed by reaction of NBT with superoxide, observed at 560 nm. As shown in Figure S1, [Cu(py$_2$pn)]$^{2+}$ inhibits the reduction of NBT, and IC_{50} = 0.56 μM (the concentration of the SOD mimic that diminishes by 50% the reduction of NBT) was obtained graphically. The IC_{50} value depends on the concentration and type of the indicator, hence cannot be compared directly to other complexes.[40] This IC_{50} value was used to calculate the *McCord−Fridovich* second-order rate constant, $k_{McF} = k_{NBT}$ [NBT]/IC_{50} = 4.05 x 10^6 M^{-1} s^{-1} (k_{NBT} = 5.94×10^4 M^{-1} s^{-1}), which is independent of the detector and suitable to compare with literature values.[41]

Table 1. SOD activity of [Cu(py$_2$pn)]$^{2+}$ and other Cu(II) complexes.

Entry	Compound	Ligand Donor sites	k_{McF} (M^{-1}s^{-1})	$E_{1/2}$ (mV vs *SCE*)	Ref.
1	CuZn-SOD (human)	N_4	~2x10^9	+156	[42]
2	Cu(Pupy)$^{2+}$	N_4	2.36 x 10^7	-	[43]
3	[Cu(PBMPA)]$^+$	N_3O	1.25x10^7	264	[44]
4	[Cu(Pu-6-MePy)(H$_2$O)]$^{2+}$	N_4	6.3x10^6	-	[45]
5	[Cu(py$_2$pn)]$^{2+}$	N_4	4.05x10^6	-39	This work
6	[Cu(PClNOL)Cl]$^+$	N_3O	3.33x10^6	-416[47]	[46]
7	[Cu(5-EtO-salpn)ZnCl$_2$]	N_2O_2	2.1x10^6	-	[48]
8	[Cu(4-OMe-salen)ZnCl$_2$]	N_2O_2	8.7x10^5	-	[49]
9	[CusalpnZnCl$_2$]	N_2O_2	8.5x10^5	-689	[50]

HPBMPA = N-propanoate-N,N-bis(2-pyridylmethyl)amine; Pu-6-MePy = N,N′-bis(2-(6-methylpyridyl)methylen)-1,4-butanediamine; PuPy = N,N′-bis(2-pyridylmethylen)-1,4-butanediamine; HPClNOL = 1-[bis(pyridin-2-ylmethyl) amino]-3-chloropropan-2-ol; salpn = 1,3-bis(salycilidenamino)propane; 4-OMe-salen = N,N'-bis(4-methoxysalicylidene)cyclohexane-1,2-diamine,

In Table 1 the SOD activity of the complex is compared to other selected Cu(II) complexes of open chain tetradentate ligands for which k_{McF} was given or could be calculated from reported data.[42-50] The [Cu(py$_2$pn)]$^{2+}$ complex exhibits intermediate activity among related Cu-based SOD-mimics. As stated before, the reactivity is influenced by the redox potential, but also, by the ligand flexibility to accommodate geometrical rearrangements when converting from tetragonal, square-pyramidal or trigonal bipyramidal coordination geometry preferred for Cu(II) to tetrahedral or three-coordinated Cu(I). [Cu(Pupy)]$^{2+}$ (PuPy = N,N′-bis(2-

pyridylmethylen)-1,4-butanediamine) with the longer and more flexible $-(CH_2)_4-$ spacer between the imine functions (entry 2, Table 1) shows higher SOD activity than $[Cu(py_2pn)]^{2+}$, probably due to the lower reorganization barrier during electron transfer.[43] However, introduction of a methyl substituent ortho to the pyridine function (entry 4),[45] reduces its activity, owing to steric hindrance. The Cu(II) complex formed with the tripodal amine PBMPA (HPBMPA = N-propanoate-N,N-bis(2-pyridylmethyl)amine, entry 3)[44] where the apical position is occupied by a carboxylate oxygen, is more active. In this case, the ligand arrangement and the redox potential have been suggested to favor the binding and electron transfer from the substrate. Replacement of carboxylate in $[Cu(PBMPA)]^+$ by an alcohol in $[Cu(PCINOL)Cl]^+$ (entry 6)[46] decreases the activity indicating that carboxylate has a role to assist the proton coupled electron transfer process. Finally, Cu(II)-Schiff base complexes with terminal phenolate groups (entries 7-9)[48-50] show lower redox potentials and are the least reactive.

$[Cu(py_2pn)]^{2+}$ reacts rapidly with KO_2 at 25ºC in DMSO, where the radical anion is both a powerful reductant and a nucleophile, and rather stable toward self-dismutation. In this solvent, the final Cu(II) species could be characterized in solution by EPR spectroscopy and ESI-MS. Reaction mixtures containing 2-10 mM KO_2 + 1 mM $[Cu(py_2pn)]^{2+}$ were frozen a few seconds after mixing, and analyzed by X-band EPR spectroscopy, at 120 K. In any case, the spectral features of the observed species were $g_{\|}$ = 2.24, $A_{\|}$ = 187 x 10^{-4} cm^{-1} and $g_{\perp}$ = 2.06, characteristic of a Cu(II) coordination geometry with a N_4-square-planar base (Figure 4 (a,b)).[16] Therefore, after reaction with $O_2^{\bullet-}$, Cu(II) ion retains the distorted square-pyramidal geometry,[26] and exhibits a well-defined N-superhyperfine (shf) pattern with a_N = 11.5 x 10^{-4} cm^{-1} in the perpendicular region of the spectrum (Figure 4, inset). The observation of the shf pattern is probably due to the higher ionic strength after addition of KO_2 that favors the formation of a good glass and thus better resolved lines.

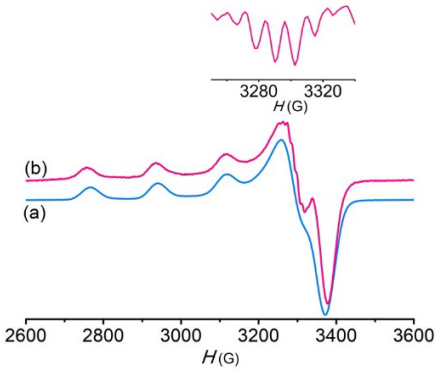

Figure 4. EPR spectra of $[Cu(py_2pn)]^{2+}$ in DMSO frozen solution (a) before and (b) after reaction with excess of KO_2. Inset: second derivative showing N-superhyperfine coupling pattern

The signal of KO_2 ($g_{\|}$ = 2.1021, $g_{\perp}$ = 2.003)[51] was never observed in the EPR spectra of the reaction mixtures indicating rapid disappearance of excess of $O_2^{\bullet-}$ catalyzed by the complex (essentially, the reaction ended before freezing). ESI-mass spectra of 5:1 and 10:1 KO_2:complex reaction mixtures in DMSO (Figure S2) confirmed the recovery of the catalyst at the end of the reaction. Notably, no ligand peak is observed, indicating the robustness of the N_4-coordinate framework of the complex during reaction.

Further evaluation of the reaction by UV−vis spectroscopy at low temperature provided evidence in support of the involvement of Cu(I) in the redox cycle. To slow down the reaction rate and observe the reduced form of the catalyst, the complex was reacted with 1.3 equiv. KO_2 stabilized with 1.4 equiv. of 18-crown-6-ether at -40ºC in 4:1 DMF:THF, and the reaction was followed by UV-vis spectroscopy, under N_2. A color change from green to brown was observed immediately after mixing, concomitantly with the change of the spectral pattern of the starting complex (Figure 5 (a,b)) that overlaps with new bands characteristic of Cu(I) (Figure 5 (c,d)). It is known that $[Cu(py_2pn)]^+$ adopts a flattened geometry, and presents two allowed electronic transitions between d_{xz} and d_{yz} orbitals of Cu(I) and two π^* orbitals of the Schiff-base ligand of the tetracoordinated metal ion, at 380 nm (ε = 3.3 x 10^3 M^{-1} cm^{-1}) and 650 nm (ε = 1.1 x 10^3 M^{-1} cm^{-1}), respectively.[29] Besides, $[Cu(py_2pn)]^+$ can dimerize and the monomer/dimer equilibrium depends on the total Cu(I) concentration.[52] In the dimer the geometrical arrangement around each Cu(I) is tetrahedral, exhibiting an intense absorption band at 460 nm (ε = 11681 M^{-1} cm^{-1}).[52]

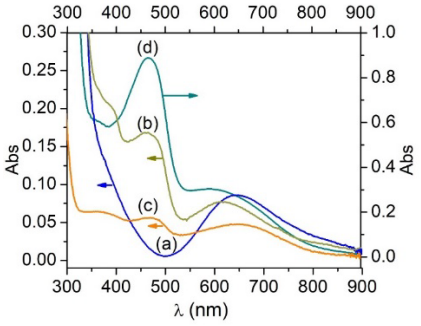

Figure 5. Electronic spectra of (a) 1 mM $Cu(py_2pn)^{2+}$ in DMF; (b) + 1.3 equiv. KO_2; (c) 50 μM $Cu(py_2pn)^{2+}$ + 1 equiv. of sodium ascorbate, in 98:2 DMF:H_2O; (d) 1 mM $Cu(py_2pn)^{2+}$ + 1 equiv. of sodium ascorbate, in 91:9 DMF:H_2O

The Cu(I) spectral features of the reaction mixture (Figure 5 (b)) evidence a mixture of the Cu(I) monomer $[Cu(py_2pn)]^+$ and dimer $[Cu(py_2pn)]_2^{2+}$, in addition to the starting Cu(II) complex. The presence of $[Cu(py_2pn)]^{2+}$, $[Cu(py_2pn)]^+$ and $[Cu(py_2pn)]_2^{2+}$ in the final reaction mixture was confirmed comparing the absorption spectrum with the product of the reduction of $[Cu(py_2pn)]^{2+}$ with ascorbate (Figure 5 (c) and (d)). In the last case, stoichiometric reduction of the starting complex occurs and the Cu(I) monomer rapidly equilibrates with its dimer. When the complex concentration is 1 mM, the Cu(I) monomer represents 25% of total Cu(I) in the solution, while when the more diluted Cu(II) complex solution was treated with ascorbate, Cu(I) monomer represents 63% of total Cu(I) in the mixture. Based on the absorption data, the composition of the final $[Cu(py_2pn)]^{2+}$ + 1.3 equiv. KO_2 reaction mixture at -40ºC was estimated as 73% $[Cu(py_2pn)]^{2+}$ + 25% $[Cu(py_2pn)]^+$ + 2% $[Cu(py_2pn)]_2^{2+}$. This result means that in these conditions, Cu(I) reacts with O_2 formed as product to partially restore the starting Cu(II) complex. Notably, at low temperature, and under nitrogen, the above species distribution remains unchanged with time, as no noticeable changes in the absorption bands were observed in subsequent UV−vis spectra, at -40ºC.

When the mixture is left under air at room temperature, the Cu(I) species disappear and the Cu(II) spectrum is restored.

The optimized structures of the distorted square-pyramidal $[Cu(II)(py_2pn)DMF]^{2+}$ and flattened tetracoordinated $[Cu(I)(py_2pn)]^{+}$ are compared in Figure 6, highlighting the structural rearrangements that must occur upon reaction of $O_2^{\bullet-}$ with $[Cu(py_2pn)]^{2+}$ (calculated geometric parameters are listed in Table S1).

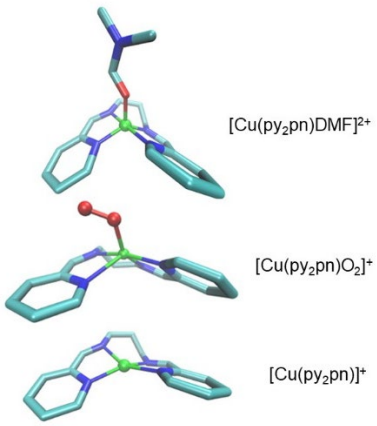

Figure 6. Calculated structures for the Cu(II) and Cu(I) complexes and the $[(py_2pn)Cu\text{-}O_2]^{+}$ adduct

DFT calculations predict $O_2^{\bullet-}$ binds the copper center with an end-on η^1-geometry (Cu-O = 1.96 Å, O-O distance = 1.27 Å and Cu-O-O angle = 121.76º, shown in Figure 6) compatible with an $[(py_2pn)CuO_2]^{+}$ adduct, where an elongated Cu-N_{py} bond of 2.45 Å renders the copper center more electrophilic and favors electron transfer from $O_2^{\bullet-}$ to the metal to yield an adduct with null Mülliken spin population on both fragments.

Reaction of $[Cu(py_2pn)]^{2+}$ with H_2O_2

$[Cu(py_2pn)]^{2+}$ is a very poor catalyst for H_2O_2 disproportionation in net protic and non protic solvents. Its low activity can be related to the redox potential of the Cu(II)/Cu(I) couple that lays outside the range of H_2O_2 oxidation and reduction at neutral pH, although if the redox reaction occurs through an inner sphere mechanism the Cu-substrate binding energy must also be considered.[53] In any case, the catalase (CAT)-like activity of $[Cu(py_2pn)]^{2+}$ improves when a base is added to the complex solution, and the redox potentials of the O_2/H_2O_2 and H_2O_2/H_2O couples become more negative encompassing the Cu(II)/Cu(I) redox potential. Therefore, the initial rate of H_2O_2 disproportionation by $[Cu(py_2pn)]^{2+}$ was measured for different complex and H_2O_2 concentrations, in the presence of Et_3N, in DMF at 25ºC (Table S2). As shown in Figure 7 (a), at constant [complex] = 1 mM, the initial rate (r_i) varies linearly with $[H_2O_2]_0$, and the first-order rate constant k_1 = 5.0(1) x 10^{-3} min^{-1} could be obtained from the slope of the straight line. At constant $[H_2O_2]_0$ = 100 mM, the reaction exhibits second-order kinetics on [catalyst], and k_2 = 498(6) M^{-1} min^{-1} was determined by non-linear fit of the plot of r_i vs $[catalyst]_0$ (Figure 7 (a)). The third-order catalytic constant k_{CAT} = 4.99(2) x 10^3 M^{-2} min^{-1} can be calculated from either $k_1/[catalyst]_0^2$ or $k_2/[H_2O_2]_0$.

When the reaction is performed in aqueous buffer of pH 7, $k_{CAT}^{pH=7}$ = 5.7 x 10^2 M^{-2} min^{-1}, while at pH 9, the reaction is much faster, and $k_{CAT}^{pH=9}$ = 1.2 x 10^6 M^{-2} min^{-1}. The CAT activity of $[Cu(py_2pn)]^{2+}$ at pH 9 is higher than that of mononuclear $[Cu(PBMPA)]^{+}$,[44] at pH 11 and $[Cu(apzpn)]^{2+}$ (apzpn = N,N'-bis(2-acetylpyrazyl)methylene-1,3-diaminopropane)[54] at pH 8. However, at pH 7, mononuclear Cu(II) complexes are much less reactive than dinuclear Cu(II) complexes, thus reinforcing the requirement of two Cu(II) centers for CAT activity.[55]

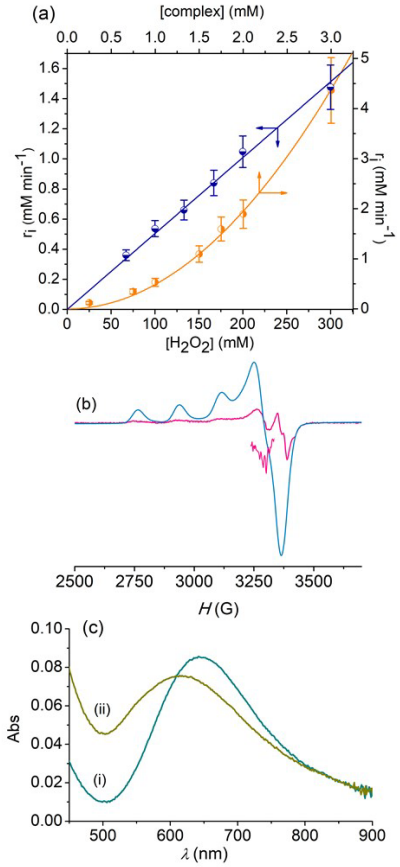

Figure 7. (a) Influence of [catalyst] and $[H_2O_2]$ on the rate of H_2O_2 disproportionation in DMF. $[Et_3N]$ = 100 mM; T = 25 ºC. (b) Compared EPR spectra of the $[Cu(py_2pn)]^{2+}$ + H_2O_2 reaction (pink line) and starting complex (blue line). Second derivative of the perpendicular region of the pink spectra is also shown. (c) d-d band of $[Cu(py_2pn)]^{2+}$ in (i) Et_3N/DMF and (ii) at the end of the reaction of a 1:25:25 complex:H_2O_2:Et_3N mixture, in DMF.

When the complex is left to react with H_2O_2 in DMF and the reaction mixture is frozen, the low-temperature X-band EPR spectrum displays the characteristic pattern of distorted square-pyramidal Cu(II) complexes (Figure 7 (b)).[16,26] Inspection of the spectrum reveals the presence of two paramagnetic species with two sets of $g_{\|}$ values with distinct $A_{\|}$. Spectral deconvolution afforded $g_{\|}^1$ = 2.25, $A_{\|}^1$ = 187 x 10^{-4} cm^{-1}, $g_{\perp}^1$ = 2.06, $g_{\|}^1/A_{\|}^1$ = 120, similar to the starting complex, and a second species with $g_{\|}^2$ = 2.23, $A_{\|}^2$ = 167 x 10^{-4} cm^{-1}, $g_{\perp}^2$ = 2.06, $g_{\|}^2/A_{\|}^2$ = 133, exhibiting N-superhyperfine coupling in the perpendicular region of the spectrum. The low intensity of the EPR signal suggests a low proportion of these paramagnetic species during the course of the reaction. At the end of the reaction in basic DMF, the starting complex is recovered together with another species with d-d band shifted towards shorter wavelength (λ_{max} = 608 nm (ε = 90 M^{-1} cm^{-1})) shown in Figure 7 (c), indicating the absence of major structural rearrangements after reaction. ESI-mass spectra registered

during or after reaction show the same peaks and fragmentation pattern as the starting solution.

The second order dependence on $[complex]_0$ indicates that a second complex molecule is involved in H_2O_2 decomposition at (or before) the slow step of the catalytic cycle. In order to gain insight into the mechanism of the reaction, mixtures of the complex with excess H_2O_2 + Et_3N in DMF were monitored by UV–visible spectroscopy at -40 ºC. The absorption spectra of these reaction mixtures show an intense band at 370 nm (ε = 905 M^{-1} cm^{-1}) that increased together with a less intense and broad d-d band at ~ 550 nm (ε = 145 M^{-1} cm^{-1}). These bands grew up and reached a maximal absorbance whose final intensity depended linearly on [complex]. Figure 8 (a) shows the successive electronic spectra for the reaction of $[Cu(py_2pn)]^{2+}$ with 10 equiv. of H_2O_2 in DMF at -40ºC in the presence of 10 equiv. of Et_3N.

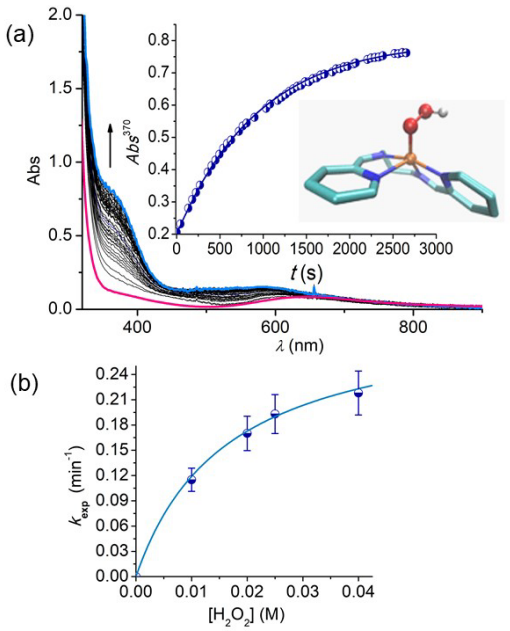

Figure 8. (a) Spectrophotometric monitoring of the formation of $[Cu(py_2pn)OOH]^+$ Conditions: 1:10:10 complex:Et_3N:H_2O_2, DMF, -40ºC. [complex] = 0.95 mM. Inset: First-order fit of Abs^{370} vs *t* data, and optimized structure for the hydroperoxo adduct. (b) Influence of $[H_2O_2]_0$ on the rate of $[Cu(py_2pn)OOH]^+$ formation.

In all the analyzed H_2O_2:complex mixtures (10:1 to 100:1 ratios), the final species remains stable over time at -40 ºC. The observed UV-vis spectral pattern is characteristic of Cu(II)-hydroperoxo complexes with square-pyramidal structure.[3,10,11] This species can account for the second EPR signal ($g_{\|}$ = 2.23, $A_{\|}$ = 167 x 10^{-4} cm^{-1}, $g_{\perp}$ = 2.06) observed in the frozen reaction mixture (Figure 7 (b)), with hydroperoxide occupying the axial position of the distorted square-pyramide.[56-58] The optimized structure of the Cu(II)-hydroperoxide adduct, shown in the inset of Figure 8 (a), confirmed the distorted square-pyramidal geometry and proved that substitution of perchlorate/solvent by hydroperoxide, a stronger donor ligand, shortens the Cu-O bond to 1.92 Å and elongates one Cu-N_{py} bond to 2.48 Å, affording a Cu-O binding energy of 47.06 kcal/mol, calculated as $E_{[Cu(py2pn)OOH]^+}$ - (E_{O2H}- + $E_{[Cu(py2pn)]^{2+}}$). Besides, the hypsochromic shift of the d-d band of the complex upon formation of the Cu(II)-hydroperoxide adduct is in agreement with the electronic transitions predicted by TD-DFT calculations. The calculated Mülliken spin population of +0.5 on copper and +0.4 on the O_2 moiety, suggests that both fragments of the Cu(II)-hydroperoxide adduct host the unpaired electron.

The growth of the absorption band of the Cu(II)-hydroperoxide adduct follows an exponential behavior, and the first-order k_{exp} was determined by fitting of Abs^{370} vs time. At constant [Et_3N], the variation of k_{exp} values with $[H_2O_2]$ (shown in Figure 8 (b) and Table S3) could be fitted to eq. 1, from which the kinetic parameters a = 3.1(7) x 10^{-1} min^{-1} and b = 1.6(8) x 10^{-2} M were obtained.

$$k_{exp} = \frac{a[H_2O_2]}{b + [H_2O_2]} \quad (1)$$

Therefore, the full kinetic law for the formation of $[Cu(py_2pn)OOH]^+$ can be written as in eq. 2:

$$r^{CuOOH+} = \frac{a\,[H_2O_2]}{b + [H_2O_2]}[complex] \quad (2)$$

Taking these experimental evidences into account, we propose an interchange mechanism as a possible pathway for reaching the Cu(II)-hydroperoxide adduct. In this mechanism, $[Cu(py_2pn)X]^{2+/+}$ (X is a coordinated solvent molecule or ClO_4^-) exchanges X by HO_2^- (formed in the presence of Et_3N), through the rapid formation of an outer sphere complex between the two oppositely charged species, as depicted in eqs. (3)-(5) of Scheme 1. For this mechanism, K_0 is known (K_0 = 7.5 x 10^2),[56-58] k^{OOH} = 0.31 min^{-1}, and K_1 = 8.3 M^{-1}, a reasonable value for an outer sphere complex between 2+ and 1+ ions.[59]

$$H_2O_2 + Et_3N \overset{K_0}{\rightleftharpoons} HO_2^- + Et_3NH^+ \quad (3)$$

$$HO_2^- + [Cu(py_2pn)X]^{2+} \overset{K_1}{\rightleftharpoons} [Cu(py_2pn)X^{2+}\text{----- }OOH^-] \quad (4)$$

$$[Cu(py_2pn)X^{2+}\text{----- }OOH^-] \xrightarrow{k^{OOH}} [Cu(py_2pn)OOH]^+ + X \quad (5)$$

Scheme 1. Proposed mechanism for $[Cu(py_2pn)O_2H]^+$ formation

Rapid ligand exchange and Cu(II)-hydroperoxide formation have already been observed for $[Cu(tmpa)]^{2+}$ under similar conditions.[60] Therefore, from kinetic data, it seems evident that the formation of the Cu(II)-hydroperoxide adduct is not the rate determining step during the catalytic H_2O_2 disproportionation, otherwise the slow step must involve a second complex molecule. On the basis of the available experimental evidence and DFT calculations, a feasible pathway for O_2 formation from the H_2O_2 + $[Cu(py_2pn)]^{2+}$ mixture in basic DMF, at room temperature, is presented in Scheme 2.

$$[Cu(py_2pn)O_2H]^+ + [Cu(py_2pn)]^{2+} \xrightarrow[-\,H^+]{k^D,\ slow} [(py_2pn)CuO_2Cu(py_2pn)]^{2+} \quad (6)$$

$$[(py_2pn)CuO_2Cu(py_2pn)]^{2+} \xrightarrow{fast} 2\,[Cu(py_2pn)]^+ + O_2 \quad (7)$$

Scheme 2. Proposed pathway for the formation of O_2 in the H_2O_2 + $[Cu(py_2pn)]^{2+}$ reaction in basic DMF at RT

It is proposed that Cu(II)-hydroperoxide formed according eqs. (3)-(5) reacts with a second Cu(II) complex in the rate determining step (eq. (6)) to give the *trans*-μ-1,2-peroxodicopper(II) complex

which rapidly yields two Cu(I) complexes and O_2 as products of the redox half-reaction of the CAT cycle, as observed for other copper complexes of N_4-tetradentate ligands.[58,61] Proton transfer to the external base favors the formation of the dimer in the slow step (supported by the extremely slow reaction without addition of base).[62] DFT calculations converged to a Cu-O_2-Cu intermediate (shown in Figure 9) with Cu-O distances of 2.04 and 2.08 Å, and O-O bond distance of 1.29 Å. The O-O distance and the Mülliken population of +1.4 on the O_2 fragment of this intermediate sustains fast electron transfer from peroxide to copper to yield the redox products.

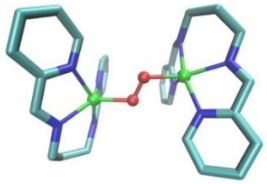

Figure 9. DFT calculated structure for the $[(py_2pn)CuO_2Cu(py_2pn)]^{2+}$ intermediate

Oxidation of phenol by H_2O_2 catalyzed by $[Cu(py_2pn)]^{2+}$

The catalytic activity of $[Cu(py_2pn)]^{2+}$ for phenol oxidation by H_2O_2 was tested in aqueous solution of pH 7. Neutral pH was selected taking into account the much higher value of k_{CAT} in basic medium, discussed above. The reaction was monitored spectrophotometrically in the presence of excess of 4-aminoantipyrine (4-AAP), by following the absorbance increase at 498 nm due to the formation of the *p*-quinoneimide (*p*-QI) adduct (ε = 7290 M^{-1} cm^{-1}).[63]

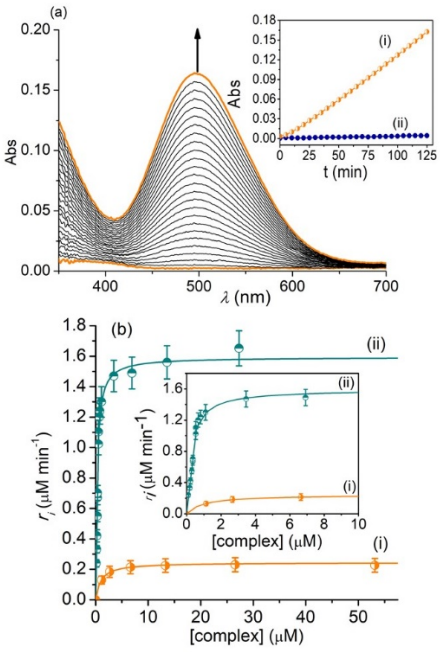

Figure 10. (a) Electronic spectra taken during H_2O_2 oxidation of phenol catalyzed by $[Cu(py_2pn)]^{2+}$, at pH 7 and 25ºC. Conditions: [phenol] = 0.27 mM, [4-APP] = 0.68 mM, $[H_2O_2]$ = 3.3 mM, [catalyst] = 0.0026 mM. Inset: Time course for product formation in the catalyzed (i) and uncatalyzed (ii) oxidation of phenol. (b) Influence of [complex] on the rate of *p*-quinonimide formation, at pH 7, (i) 25ºC and (ii) 50ºC. [phenol] = $[H_2O_2]$ = 0.27 mM, [4-APP] = 0.68 mM. *Inset*: Zoom of initial rates for [complex] < 10 μM.

As evident from Figure 10 (a), at pH 7, the complex catalyzes the H_2O_2 oxidation of phenol to the quinone, at 25ºC. In these conditions, the uncatalyzed oxidation of phenol by H_2O_2 is much slower, as shown in the inset of Figure 10 (a). To accelerate the catalyzed reaction rate, the phenol oxidation was performed at 50ºC, and, effectively, turnover frequencies (*TOF* = mol *p*-QI/mol catalyst h) increased from 4 to 29 h^{-1}, keeping pH = 7, 100-times excess of reagents over catalyst, and [complex] = 2.6 μM. Higher *TOF*s with increasing temperature had already been observed for phenol oxidation catalyzed by Cu(II) complexes of salen-type Schiff-base ligands at T > 60ºC,[64-66] and tetrazamacrocycle ligands in basic medium and 80ºC.[67] Aimed at determining if mono- or dicopper species are required for peroxidase activity of $[Cu(py_2pn)]^{2+}$, the initial rate for the formation of the *p*-QI (r_i^P) was measured from the growth of absorbance at 498 nm for different complex concentrations, maintaining constant $[H_2O_2]_0$ = $[phenol]_0$ = 0.27 mM, at 25ºC and 50ºC (Table S4). As shown in Figure 10 (b), r_i^P exhibits saturation kinetics with $[complex]_0$ and could be fitted to the equation (8):

$$r_i^P = \frac{c\,[complex]}{d+[complex]} \qquad (8)$$

from which kinetic parameters c = 8.7(1) x 10^{-4} μM min^{-1} and d = 0.7(8) μM, at 25ºC, and c = 5.9(6) x 10^{-3} μM min^{-1} and d = 0.26(6) μM, at 50ºC, were determined.

This rate law can be interpreted by the mechanism presented in equations (9) – (11) of Scheme 3, where inhibition by the complex is related to the CAT activity of the peroxo dimer (*vide supra*). The first step in this reaction is proposed to be the formation of the Cu(II)-hydroperoxide adduct that can either oxidize phenol to yield the observed *p*-QI, or react with a second Cu(II) complex to afford O_2 and the reduced complex through the trans-μ-1,2-peroxo-dimer intermediate as discussed in the previous section.

$$H_2O_2 + [Cu(py_2pn)]^{2+} \xrightarrow{k^a} [Cu(py_2pn)OOH]^+ + H^+ \qquad (9)$$

$$[Cu(py_2pn)OOH]^+ \xrightarrow[+\ phenol,\ 4\text{-}AAP]{k^{QI}} p\text{-quinoneimide} + [Cu(py_2pn)OH]^+ + H_2O \qquad (10)$$

$$\xrightarrow[+\ [Cu(py_2pn)]^{2+}]{k^c} 2\ Cu(py_2pn)]^+ + H^+ + O_2 \qquad (11)$$

Scheme 3. Proposed reaction pathway for phenol oxidation.

If $[Cu(py_2pn)O_2H]^+$ is assumed to be in steady state, experimental kinetic parameters can be expressed as: c = $k^{a'}$ $k^{QI'}$ /k^c, and d = $k^{QI'}/k^c$, where $k^{a'} = k^a \cdot f[H_2O_2]_0$, $k^{QI'} = k^{QI} \cdot f[phOH]_0$, with $[H_2O_2]$ and [phOH] kept constant in all measurements. The calculation of $k^{a'}$ from the c/d ratio at both temperatures, affords an estimated activation energy of 22.3 kcal/mol for the formation of the Cu(II)-hydroperoxide. From this value, the first-order rate constant predicted for the Cu(II)-hydroperoxide formation in an aqueous solution of pH 7, at -40ºC is $k^{a'(-40ºC)}$ = 3.44 x 10^{-6} min^{-1}, a value much lower than for the base catalyzed formation in DMF/Et_3N that confirms the role played by the base to favor HO_2^- binding to Cu(II).

In the mechanism of Scheme 3, the mononuclear Cu(II)-hydroperoxide is the oxidant for phenol oxidation[1] (equation (10)) as recently found for H_2O_2 oxidation of serotonin catalyzed by Cu(II)-$A\beta$.[68] Discrete mononuclear Cu(II)-hydroperoxide

complexes have also been found to mediate the aryl hydroxylation and amine oxidative N-dealkylation by Cu(II) complexes of tmpa derivatives (tmpa = tris(2-pyridylmethyl)amine), although through different mechanisms.[69,70] The phenol oxidation step of equation 10 may involve binding of phenol to the metal center to form a ternary $[Cu(py_2pn)(O_2H)(phOH)]^+$ transition state where the bound substrate converts into the product.[3] On the basis of DFT calculations, binding of phenol to the copper center might occur with one N_{py}-Cu bond cleavage (one N_{py} of the ligand sits at 2.93 Å from copper) and adoption of a trigonal bipyramidal geometry with phenol occupying an equatorial position, as shown in Figure 11, with distances and angles listed in Table S1, for which the calculated $\Delta G^{\#}$ is 10.52 kcal/mol. Thus, N-decoordination plus reorganization energy of the copper center might slow down the formation of the $[CuOOH(phOH)]^+$ transition state, while H bonding of the HO group of phenol to the distal O atom of the $[CuOOH]^+$ lengthens the O−O bond ($d_{O\text{-}O}$ = 1.46 Å) favoring O-O bond scission along with electron transfer, probably through a concerted mechanism.[3,5]

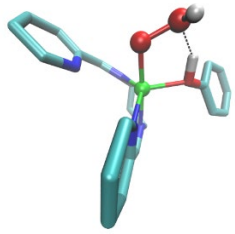

Figure 11. Proposed structure for a ternary $[Cu(N_3\text{-}py_2pn)(O_2H)(phOH)]^+$ transition state in phenol oxidation.

Only when [complex] < $k^{QI'}/k^c$, phenol oxidation is favored *vs* O_2 formation, thus explaining the higher turnover numbers achieved when diluted catalyst solutions are employed. The interaction of the Cu(II)-hydroperoxide intermediate with the second Cu(II) complex (eq. (11)) occurs through the *trans*-μ-1,2-peroxodicopper(II) complex, which is poorly reactive toward phenol oxidation.[71,72] Instead, side-on peroxo-bridged dicopper(II) complexes have proved ability for phenol oxidation at room temperature,[71-74] and phenol hydroxylation at low temperature.[72,75,76] In the present case, DFT calculations demonstrate that the formation of the μ^2-η^2:η^2-peroxodicopper(II) complex is not favored energetically. Even starting from the side-on peroxo-bridged complex, calculations converge to the *trans*-1,2-peroxo bridged isomer, which, as discussed in the previous section, evolves O_2 and yields two Cu(I) complexes through fast electron transfer, thus, supporting the higher *TONs* achieved for phenol oxidation as the complex concentration decreases.

Conclusion

$[Cu(py_2pn)]^{2+}$ has shown high versatility to react with reduced forms of O_2 and catalyze phenol oxidation proving SOD, CAT and peroxidase activities, although with different efficacy. In the solid state, the neutral complex $[Cu(py_2pn)(ClO_4)_2]$ exhibits an elongated tetragonal geometry with the two perchlorate anions bound to Cu(II) in the axial positions. However, in solution the complex cation $[Cu(py_2pn)X]^{+/2+}$ (X = ClO_4^- or solvent) adopts a distorted square-pyramidal geometry with one perchlorate or a solvent molecule at the apex. $[Cu(py_2pn)]^{2+}$ is competent to scavenge $O_2^{\bullet-}$ employing a Cu(II)/Cu(I) redox cycle for SOD activity. The reactivity of the complex is related to the flattened geometry adopted by the tetradentate ligand around the Cu(I) atom close to the geometry of the starting Cu(II), except for the position of one N_{py} donor site that moves nearer the equatorial plane in the reduced complex. DFT calculations suggest that even when py_2pn is not a very flexible ligand, elongation of one of the N_{py} binding sites provides a path for fast electron transfer from superoxide to a more electrophilic Cu(II) center to afford Cu(I) without much energetic cost. Therefore, the reaction is fast even at -40ºC, where $[Cu(py_2pn)]^+$ and its dimer could be observed in a 1:1 Cu(II):$O_2^{\bullet-}$ reaction mixture. Otherwise, the CAT activity of $[Cu(py_2pn)]^{2+}$ is much lower, is favored in basic conditions where the H_2O_2 reduction and oxidation potentials become more negative encompassing the Cu(II)/Cu(I) redox couple, and involves a second complex molecule to yield the redox products through a two-electron redox cycle. In this case, the first step involves a distorted square-pyramidal end-on Cu(II)-hydroperoxide intermediate which then reacts with other Cu(II) complex to yield the redox products most probably through the *trans*-μ-1,2-peroxodicopper(II) species. DFT calculations show the end-on Cu(II)-hydroperoxide can react with another Cu(II) complex through proton dissociation and distal oxygen nucleophilic attack. This is in line with the recently reported nucleophilic reactivity of Cu(II)-hydroperoxide.[14] In the peroxo-bridged dimer, each Cu(II) center possesses a square-pyramidal geometry and the elongation of one of the N_{py} coordination sites facilitates electron transfer from peroxide to the metal centers to yield the flattened tetracoordinated Cu(I), as confirmed by the Mülliken populations in the O_2 fragment of the dimer. It is also proposed that the end-on Cu(II)-hydroperoxide can mediate phenol oxidation, although larger geometry reorganization around the Cu(II) center (including N_{py}-Cu bond dissociation) is required to form a trigonal bipyramidal ternary transition state for electron transfer, resulting in slow phenol oxidation kinetics, favored over CAT activity when low proportion of catalyst is used.

Experimental Section

The reagents and solvents used in this study were commercial products of the highest available purity and were further purified by standard methods, as necessary.

Synthesis of ligand and complex. Py_2pn was synthesized following the procedure previously reported in ref. [77]. $[Cu(py_2pn)(ClO_4)_2]$ was synthesized by using $Cu(OAc)_2$ and then adding $NaClO_4$, a method different from previously reported.[30,31] Synthetic details for the obtention of these compounds are described in the Supporting Information.

SOD activity indirect assay. The SOD-like activity of the complexes was evaluated by measuring the inhibition of the reduction of NBT by $O_2^{\bullet-}$ spectrophotometrically.[38] The reaction mixtures contained riboflavin (3.35×10^{-6} M), methionine (9.52×10^{-3} M), NBT (3.82×10^{-5} M), and complex (different concentrations), in phosphate buffer (pH 7.8). Riboflavin was added last and the mixtures were illuminated during 15 min with an 18 W fluorescent lamp placed at 15 cm, at 25 °C. The reduction of NBT was measured at 560 nm, and the IC_{50} values were determined graphically. Control reactions confirmed that the compounds did not react directly with NBT or riboflavin. Inhibition percentage was calculated according to: $\{(\Delta Abs/t)_{without\ complex} - (\Delta Abs/t)_{with\ complex}\} \times 100/(\Delta Abs/t)_{without\ complex}$.

Preparation of potassium superoxide solutions. For EPR and ESI-MS measurements, stock KO_2 solution in anhydrous DMSO was prepared by mixing 9.3 mg of KO_2 in DMSO (5 mL) and sonicated for 15 min, followed by centrifugation at 6000 rpm during 25 min. The concentration of KO_2 in the supernatant was estimated by using its extinction coefficient 2686 M^{-1} cm^{-1} in deoxygenated DMSO solution[78] and confirmed by the horseradish peroxidase assay.
For UV-vis measurements, KO_2 solutions were prepared by placing 1 equivalent of KO_2 and 1.4 equivalents of 18-crown-6 ether and dissolving in cold DMF to the desired concentration, stirred for 10 min and filtered through a nylon membrane. The solution was then diluted with DMF/THF to a final 2 mM concentration in 1:4 THF:DMF. After cooling at -40ºC in an acetonitrile/dry ice bath under N_2, an equal volume of 2 mM $[Cu(py_2pn)]^{2+}$ solution in 1:4 THF:DMF was added, and the spectra registered with a Hellma UV-vis immersion probe.

Evaluation of CAT activity. Reaction rates were determined by volumetric measurement of the O_2 evolved after addition of excess of H_2O_2 to a DMF solution of the complex containing 100 mM Et_3N. A round-bottom flask with a rubber septum, containing the degassed solution of the complex, was thermostated at 25 ºC and connected to a gas-measuring burette (precision of 0.1 mL). Previously thermostated H_2O_2 was injected through the septum to the stirred complex solution, and the evolved O_2 was measured with the burette. The initial reaction rates were obtained by fitting the $[O_2]$ versus time data to a polynomial expression and calculating the slope of the tangent at time zero. Each rate constant reported here represents the mean value of multiple determinations that fall within ±5%. All experiments were carried out at 25 ºC. Blanc experiments performed with 100 mM H_2O_2 and 100 mM Et_3N in DMF without the catalyst showed less than 2% decomposition after 2 h and measured values were deducted from catalytic measurements.

UV-vis monitoring of the $[Cu(py_2pn)OOH]^+$ formation at -40ºC. The deoxygenated complex solution in DMF (1 mM) was kept with stirring for several minutes a -40ºC, and then a cold solution of excess H_2O_2 + Et_3N in DMF (previously thermostated at -40ºC) was injected through a septa cap, and the reaction monitored by following the increase of absorbance at 370 nm.

Measurement of peroxidase activity. In a typical experiment, 10 μL of a 0.99 M H_2O_2 in acetone were added to 2.5 mL of phosphate buffer containing 0.80 μmol of phenol and 2.04 μmol of 4-aminoantipyrine (4-AAP). The reaction started with addition of 0.5 mL of solutions of different complex concentrations in DMF, with stirring. The reaction was monitored by following absorption band at 498 nm during 2 h, at 25ºC and 50ºC. Control reaction was performed by mixing all reagents except the complex. Molar absorption coefficient of the *p*-quinoneimide adduct at 498 nm (ε = 7290 M^{-1} cm^{-1}) was determined by complete oxidation of phenol by horseradish peroxidase (200 UI/mL), under the same experimental conditions.

Physical Measurements. UV−visible spectra were recorded on a Jasco V-550 spectrophotometer, with thermostated cell compartments. Measurements at -40ºC were conducted with a Hellma immersion probe. EPR spectra were obtained at 120 K on an Elexsys E 500 Bruker spectrometer, operating at a microwave frequency of approximately 9.5 GHz. IR spectra were recorded on a PerkinElmer Spectrum One FT-IR spectrophotometer. Metal content was determined with an Inductively coupled plasma mass spectrometer (ICP-MS) Perkin Elmer NexION 350×. ESI-mass spectra were obtained with a Thermo Scientific LCQ Fleet. The solutions for electrospray were prepared from solutions of the complexes diluted with methanol to a ≈ 10^{-5} M concentration. ^{1}H NMR spectra were recorded on a Bruker AC 300 NMR spectrometer at ambient probe temperature (ca. 26 °C). Chemical shifts are referenced to $(CH_3)_4Si$ (^{1}H NMR) and downfield shifts are given a positive sign. Paramagnetic NMR spectra were acquired using super WEFT sequence, with acquisition time of 15 ms. The electrochemical experiments were performed with a computer-controlled Princeton Applied Research potentiostat, VERSASTAT II model, with the 270/250 Research Electrochemistry Software. Studies were carried out under Ar, in DMF solution using 0.1 M Bu_4NPF_6 as a supporting electrolyte and ≈ 10^{-3} M complex. The working electrode was a Pt wire, and the reference electrode was a calomel electrode isolated in a fritted bridged with a Pt wire as the auxiliary electrode. Under these conditions, *E*(ferrocene/ferrocenium) = 474 mV, in DMF.

Computational calculations. All calculations were performed using the hybrid B3LYP[79] functional as implemented in the Gaussian 09 package.[80] This functional was used successfully in theoretical studies that involve copper complexes.[14,81,82] In this work we have employed the 6-31G** basis set for the first-row to the third-row atoms and LANL2DZ ECP for Cu atom.[83,84] The solvent effects were computed by the polarizable continuum model (PCM)[85] with the dimethylformamide DMF dielectric constant. All the optimized structures are proved to be local minima using frequency calculations. Minimized and TS structures were confirmed by analysis of the vibrational frequencies.

Acknowledgements

This work was supported by the National University of Rosario (PIP BIO553), the Consejo Nacional de Investigaciones Científicas y Técnicas (CONICET, PIP 0337 and PUE 0068), the Centre National de la Recherche Scientifique (CNRS, PICS 07121), and the Agencia Nacional de Promoción Científica y Tecnológica (ANPCyT PICT-2019-03276).

Keywords: copper • kinetics • peroxide • reactive intermediates • superoxide

[1] R. Trammell, K. Rajabimoghadam, I. Garcia-Bosch, *Chem. Rev*. **2019**, *119*, 2954-3031.
[2] K. S. M. Salih, A. M. Shraim, S. R. Al-Mhini, R. E. Al-Soufi, I. Warad, *Emergent Mater.* **2021**, *4*, 423–434.
[3] C. E. Elwell, N. L. Gagnon, Benjamin D. Neisen, D. Dhar, A. D. Spaeth, G. M. Yee, W. B. Tolman, *Chem. Rev*. **2017**, *117*, 2059-2107.
[4] S. Itoh, *Acc. Chem. Res*. **2015**, *48*, 2066-2074.
[5] D. Bailey, D. Dhar, A. C. Cramblitt, W. B. Tolman, *J. Am. Chem. Soc*. **2019**, *141*, 5470-5480.
[6] E. I. Solomon, D. E. Heppner, E. M. Johnston, J. W. Ginsbach, J. Cirera, M. Qayyum, M. T. Kieber-Emmons, C. H. Kjaergaard, R. G. Hadt, L. Tian, *Chem. Rev*. **2014**, *114*, 3659–3853.
[7] D. E. Diaz, M. Bhadra, K. D. Karlin, *Inorg. Chem.* **2019**, *58*, 13746–13750.
[8] S. Fukuzumi, Y.-M. Lee, W. Nam, *Dalton Trans*. **2019**, *48*, 9469–9489.
[9] S. Kim, C. Saracini, M. A. Siegler, N. Drichko, K. D. Karlin, *Inorg. Chem*. **2012**, *51*, 12603−12605.
[10] M. Bhadra, J. Y. C. Lee, R. E. Cowley, S. Kim, M. A. Siegler, E. I. Solomon, K. D. Karlin, *J. Am. Chem. Soc*. **2018**, *140*, 9042-9045.
[11] A. Wada, M. Harata, K. Hasegawa, K. Jitsukawa, H. Masuda, M. Mukai, T. Kitagawa, H. Einaga, *Angew. Chem., Int. Ed*. **1998**, *37*, 798-799.
[12] S. Biswas, A. Dutta, M. Debnath, M. Dolai, K. K. Das, M. Ali, *Dalton Trans*. **2013**, *42*, 13210–13219.
[13] K. M. Carsch, A. Iliescu, R. D. McGillicuddy, J. A. Mason, T. A. Betley, *J. Am. Chem. Soc*. **2021**, *143*, 18346–18352.
[14] B. Kim, D. Jeong, T. Ohta, J. Cho, *Commun Chem* **2019**, *2*, 81, doi.org/10.1038/s42004-019-0187-3.
[15] J. Y. Lee, R. L. Peterson, K. Ohkubo, I. Garcia-Bosch, R. A. Himes, J. Woertink, C. D. Moore, E. I. Solomon, S. Fukuzumi, K. D. Karlin, *J. Am. Chem. Soc*. **2014**, *136*, 9925-9937.
[16] S. Muthuramalingam, K. Anandababu, M. Velusamy, R. Mayilmurugan, *Inorg. Chem*. **2020**, *59*, 5918−5928.
[17] L. M. Mirica, X. Ottenwaelder, T. D. P. Stack, *Chem Rev*. **2004**, *104*, 1013-1045.

[18] A. Zoubi, Y. G. Ko, *J. Organomet. Chem.* **2016**, *822*, 173−188.
[19] K. C. Weerasiri, A. E. V. Gorden *Tetrahedron* **2014**, *70*, 7962-7968.
[20] O. V. Nesterova, D. S. Nesterov, A. Krogul-Sobczak, M. F. C. Guedes da Silva, A. J. L. Pombeiro, *J. Mol. Catal. A: Chem.* **2017**, *426*, 506–515.
[21] M. M. Conejo, P. Ávila, E. Álvarez, A. Galindo, *Inorg. Chim. Acta* **2017**, *455*, 638-644.
[22] E. Safaei, H. Bahramib, A. Pevec, B. Kozlevčar, Z. Jagličić, *J. Mol. Struct.* **2017**, *1133*, 526-533.
[23] N. Benferrah, M. Hammadi, C. Philouze, F. Berthiol, F. Thomas, *Inorg. Chem. Commun.* **2016**, 72, 17–22.
[24] A. Abdolmaleki, S. R. Adariani, *Catal. Commun.* **2015**, *59*, 97–100.
[25] N. W. G. Smits, B. van Dijk, I. de Bruin, S. L. T. Groeneveld, M. A. Siegler, D. G. H. Hetterscheid, *Inorg. Chem.* **2020**, *59***,** 16398−16409.
[26] B. A. Vaughn, A. M. Brown, S. H. Ahn, J. R. Robinson, E. Boros, *Inorg. Chem*. **2020**, *59*, 16095−16108.
[27] J. Stanek, A. Hoffmann, S. Herres-Pawlis, *Coord. Chem. Rev*. **2018**, *365*, 103-121.
[28] W. R. Hagen, *Metallomics* **2019**, *11*, 1768–1778.
[29] L. Llanos, C. Vera, A. Vega, D. Aravena, L. Lemus, *Inorg. Chem*. **2020**, *59*, 15061−15073.
[30] M. S. Ray, R. Bhattacharya, S. Chaudhuri, L. Righi, G. Bocelli, G. Mukhopadhyay, A. Ghosh, *Polyhedron* **2003**, *22*, 617-624.
[31] A. Jäntti, K. Rissanen, J. Valkonen, Acta Chem. Scand., 52, 1998, 1010-1016.
[32] H. Lavanant, H. Virelizier, Y. Hoppilliard, *J. Am. Soc. Mass Spectrom*. **1998**, *9*, 1217–1221.
[33] N. Ségaud, J. McMaster, G. van Koten, M. Albrecht, *Inorg. Chem.* **2019**, *58*, 16047−16058.
[34] X. A. Kunishita, J. D. Scanlon, H. Ishimaru, K. Honda, T. Ogura,M. Suzuki, C. J. Cramer, S. Itoh, *Inorg. Chem*. **2008**, *47*, 8222-8232.
[35] P. S. Subramanian, E. Suresh, P. Dastidar, S. Waghmode, D. Srinivas, *Inorg. Chem.* **2001**, *40*, 4291-4301.
[36] M. Kose, G. Ceyhan, D. Karakas. *J. Coord. Chem.* **2016**, *69*, 497-507.
[37] I. Szekacs, P. Tokarz, R. Horvath, K. Kovacs, A. Kubas, M. Shimura, J. Brasun, V. Murzin, W. Caliebe, Z. Szewczuk, A. Paluch, L. Wojnárovits, T. Tóth, J. S. Pap, Ł. Szyrwiel, *Chem. Biol. Interact.* **2019**, *306*, 78–88.
[38] C. Policar, in Redox Active Therapeutics, eds. J. S. Reboucas, I. Batinic-Haberle, I. Spasojevic, D. S. Warner and D. St. Clair, Springer, **2016,** ch. 17, pp. 125- 164.
[39] C. Beauchamp, I. Fridovich, *Anal. Biochem*. **1971**, 44, 276−287.
[40] S. Durot, C. Policar, F. Cisnetti, F. Lambert, J. P. Renault, G. Pelosi, G. Blain, H. Korri-Youssoufi, J. P. Mahy, *Eur. J. Inorg. Chem.* **2005**, 3513–3523.
[41] Z.-R. Liao, X.-F. Zheng, B.-S. Luo, L.-R. Shen, D.-F. Li, H.-L. Liu, W. Zhao, *Polyhedron* **2001**, *20*, 2813−2821.
[42] I. A. Abreu, D. E. Cabelli, *Biochim. Biophys. Acta* **2010**, *1804*, 263–274.
[43] J. Müller, K. Felix, C. Maichle, E. Lengfelder, J. Strähle, U. Weser, *Inorg. Chim. Acta* **1995**, *233*, 11-19.
[44] J. S. Pap, B. Kripli, I. Bors, D. Bogáth, M. Giorgi, J. Kaizer, G. Speier, *J. Inorg. Biochem.* **2012**, *117*, 60−70.
[45] J. Müller, D. Schübl, C. Maichle-Mössmer, J. Strähle, U. Weser, *J. Inorg. Biochem*. **1999**, *75*, 63–69.
[46] T. P. Ribeiro, C. Fernandes, K. V. Melo, S. S. Ferreira, J. A. Lessa, R. W.A. Franco, G. Schenk, M. D. Pereira, A. Horn Jr, *Free Rad. Biol. Med*. **2015**, *80*, 67–76.
[47] C. Fernandes, G. L. Parrilha, J. A. Lessa, L. J. M. Santiago, M. M. Kanashiro, F. S. Boniolo, A. J. Bortoluzzi, N. V. Vugman, M. H. Herbst, A. Horn Jr, *Inorg. Chim. Acta* **2006**, *359*, 3167–3176.
[48] C. Wang, S. Li, D.-J. Shang, X.-L. Wang, Z.-L. You, H.-B. Li, *Bioorg. Med. Chem. Lett*. **2011**, *21*, 4320–4324.
[49] Z.-L. You, L.-L. Ni, P. Hou, J.-C. Zhang, C. Wang, *J. Coord. Chem*. **2010**, *63*, 515–523.
[50] V. A. Daier, E. Rivière, S. Mallet-Ladeira, D. M. Moreno, C. Hureau, S. R. Signorella, *J. Inorg. Biochem*. **2016**, *163*, 162–175.
[51] R. N. Bagchi, A. M. Bond, F. Scholz, R. Stoesser, *J. Am. Chem. Soc.* **1989**, *111*, 8270−8271.
[52] L. Lemus, D. E. Díaz, L. Llanos, P. Arce, R. Lorca, J. Guerrero, J. Costamagna, D. Aravena, G. Ferraudi, A. Oliver, A. G. Lappin, *Chem. Eur. J*. **2018**, *24*, 13839-13849.
[53] C. Palopoli, J. Ferreyra, A. Conte-Daban, M. Richezzi, A. Foi, F. Doctorovich, E. Anxolabéhère-Mallart, C. Hureau, S. R. Signorella, *ACS Omega* **2019**, *4*, 48-57.
[54] M. L. Pires dos Santos, A. Faljoni-Alàrio, A. S. Mangrich, A. M. da Costa Ferreira, *J. Inorg. Biochem.*, **1998**, *71*, 71-78.
[55] A. Squarcina, A. Santoro, N. Hickey, R. De Zorzi, M. Carraro, S. Geremia, M. Bortolus, M. Di Valentin, M. Bonchio, *ACS Catal*. **2020**, *10*, 7295-7306.
[56] A. Kunishita, M. Kubo, H. Ishimaru, T. Ogura, H. Sugimoto, S. Itoh, *Inorg. Chem*. **2008**, *47*, 12032-12039.
[57] D. Maiti, A. A. Narducci Sarjeant, K. D. Karlin Inorg. Chem. 47, 2008, 8736-8747.
[58] T. Osako, S. Nagatomo, T. Kitagawa, C. J. Cramer, S. Itoh, *J. Biol. Inorg. Chem.* **2005**, *10*, 581–590.
[59] R. G. Wilkins, *Kinetics and Mechanism of Reactions of Transition Metal Complexes*, Wiley-VCH Verlag GmbH & Co., Weinheim, **2002**, pp 206-210.
[60] S. Kakuda, R. L. Peterson, K. Ohkubo, K. D. Karlin, S. Fukuzumi, *J. Am. Chem. Soc*. **2013**, *135*, 6513-6522.
[61] R. R. Jacobson, Z. Tyeklar, A. Farooq, K. D. Karlin, S. Liu, J. Zubieta, *J. Am. Chem. Soc*. **1988**, *110*, 3690-3692.
[62] Z. Tyeklár, R. R. Jacobson, N. Wei, N. N. Murthy, J. Zubieta, K. D. Karlin, *J. Am. Chem. Soc*. **1993**, *115*, 2677−2689.
[63] R. R. Carballo, V. Campodall'Orto, I. N. Rezzano, *J. Mol. Catal. A: Chem*. **2008**, *280*, 156–163.
[64] A. Mobinikhaledi, M. Zendehdel, P. Safari, *Transition Met. Chem*. **2014**, *39*, 431-442.
[65] E. Karakhanov, A. L. Maximov, Y. S. Kardasheva, V. A. Skorkin, S. V. Kardashev, E. A. Ivanova, E. Lurie-Luke, J. A. Seeley, S. L. Cron, *Ind. Eng. Chem. Res*. **2010**, *49*, 4607-4613.
[66] S. Deshpande, D. Srinivas, P. Ratnasamy, *J. Catal.* **1999**, *188*, 261-269.
[67] V. P. Bansal, R. Kumar, S. Prasad, Niraj, *J. Mol. Catal. A: Chem.* **2008**, *284*, 69-76.
[68] A. K. Nath, A. Ghatak, A. Dey, S. G. Dey, *Chem. Sci.* **2021**, *12*, 1924-1929.
[69] D. Maiti, H. R. Lucas, A. A. Narducci Sarjeant, K. D. Karlin, *J. Am. Chem. Soc.* **2007**, *129*, 6998-6999.
[70] S. Kim, J. W. Ginsbach, J. Y. Lee, R. L. Peterson, J. J. Liu, M. A. Siegler, A. A. Sarjeant, E. I. Solomon, K. D. Karlin *J. Am. Chem. Soc.* **2015**, *137*, 2867-2874.
[71] E. A. Lewis, W. B. Tolman, *Chem. Rev.* **2004**, *104*, 1047-1076
[72] M. Rolff, J. Schottenheim, H. Decker, F. Tuczek, *Chem. Soc. Rev*. **2011**, *40*, 4077–4098.
[73] A. Hoffmann, C. Citek, S. Binder, A. Goos, M. Rübhausen, O. Troeppner, I. Ivanovic´-Burmazovic´, E. C. Wasinger, T. D. P. Stack, S. Herres-Pawlis, *Angew. Chem. Int. Ed.* **2013**, *52*, 5398 –5401.
[74] J. N. Hamann, F. Tuczek, *Chem. Commun.* **2014**, *50*, 2298-2300.
[75] S. Palavicini, A. Granata, E. Monzani, L. Casella, *J. Am. Chem. Soc.* **2005**, *127*, 18031-18036.
[76] C. Citek, S. Herres-Pawlis, T. D. P. Stack, *Acc. Chem. Res.* **2015**, *48*, 2424-2433.
[77] I. I. Ebralidze, G. Leitus, L. J. W. Shimon, Y. Wang, S. Shaik, R. Neumann, *Inorg. Chim. Acta* **2009**, *362*, 4713–4720.
[78] K. Hyland, C. Auclair, *Biochem. Biophys. Res. Commun.* **1981**, *102*, 531−537.
[79] A. D. Becke, *J. Chem. Phys.* **1993**, *98*, 5648-5652.
[80] *Gaussian 09, Revision C.01*, M. J. Frisch, G. W. Trucks, H. B. Schlegel, G. E. Scuseria, M. A. Robb, J. R. Cheeseman, G. Scalmani, V. Barone, B. Mennucci, G. A. Petersson, H. Nakatsuji, M. Caricato, X. Li, H. P. Hratchian, A. F. Izmaylov, J. Bloino, G. Zheng, J. L. Sonnenberg, M. Hada, M. Ehara, K. Toyota, R. Fukuda, J. Hasegawa, M. Ishida, T. Nakajima, Y. Honda, O. Kitao, H. Nakai, T. Vreven, J. A. Montgomery, Jr., J. E. Peralta, F. Ogliaro, M. Bearpark, J. J. Heyd, E. Brothers, K. N. Kudin, V. N. Staroverov, T. Keith, R. Kobayashi, J. Normand, K. Raghavachari, A. Rendell, J. C. Burant, S. S. Iyengar, J. Tomasi, M. Cossi, N. Rega, J. M. Millam, M. Klene, J. E. Knox, J. B. Cross, V. Bakken, C. Adamo, J. Jaramillo, R. Gomperts, R. E. Stratmann, O. Yazyev, A. J. Austin, R. Cammi, C. Pomelli, J. W. Ochterski, R. L. Martin, K. Morokuma, V. G. Zakrzewski, G. A. Voth, P. Salvador, J. J. Dannenberg, S. Dapprich, A. D.

Daniels, O. Farkas, J. B. Foresman, J. V. Ortiz, J. Cioslowski, D. J. Fox, *Gaussian, Inc., Wallingford CT,* **2010**.
[81] A. W. Schaefer, A. C. Roveda Jr., A. Jose, E. I. Solomon, *J. Am. Chem. Soc*. **2019**, *141*, 10068−10081.
[82] A. W. Schaefer, M. T. Kieber-Emmons, S. M. Adam, K. D. Karlin, E. I. Solomon, *J. Am. Chem. Soc*. **2017**, *139*, 7958−7973.
[83] G. A. Petersson, M. A. Al-Laham, *J. Chem. Phys.* **1991**, *94*, 6081-6090.
[84] P. J. Hay, W. R. Wadt, *J. Chem. Phys.* **1985**, *82*, 270-283.
[85] J. Tomasi, B. Mennucci, E. Cancès, *J. Mol. Struct. (Theochem)* **1999**, *464*, 211–226.

Entry for the Table of Contents

Graphic for Table of Contents

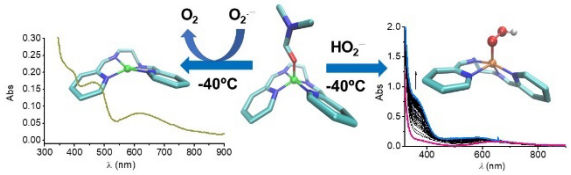

At -40ºC, the Cu(II) complex of N,N'-bis(pyridin-2-ylmethylene)propane-1,3-diamine (py_2pn) is rapidly reduced by $O_2^{\bullet-}$ to $[Cu(py_2pn)]^+$, while reacts with HO_2^- to give a stable $[Cu(py_2pn)OOH]^+$ adduct, which at room temperature reacts with $[Cu(py_2pn)]^{2+}$ evolving O_2 or oxidizes phenol when the complex is in low proportion in the reaction mixture.

Institute and/or researcher Twitter usernames: @IQUIR-CONICET; @srsignorella